RSC Advances

PAPER

View Article Online
View Journal | View Issue

Cite this: *RSC Adv.*, 2021, **11**, 198

Direct photoelectrochemical oxidation of hydroxymethylfurfural on tungsten trioxide photoanodes†

Charles R. Lhermitte,‡ Nukorn Plainpan,‡ Pamela Canjura, Florent Boudoire and Kevin Sivula *

Received 25th November 2020
Accepted 30th November 2020

DOI: 10.1039/d0ra09989a

rsc.li/rsc-advances

An important target reaction for solar-powered biomass valorization is the conversion of 2,5-hydroxymethylfurfural (HMF) into key monomers for polyester production. Herein, photoanodes of WO_3 are demonstrated to directly photo-oxidize HMF in aqueous electrolyte (pH 4) under simulated solar illumination. The addition of 5 mM HMF increases the saturation photocurrent by 26% and suppresses the water oxidation reaction, as determined by rotating ring-disk electrode experiments. Prolonged photoelectrochemical oxidation (64 h) illustrates system robustness and confirms the production of furandicarboxaldehyde (DFF), furandicarboxylic acid (FDCA), and related intermediates. Quantification of the reaction rate constants *via* a kinetic model gives insight into the modest DFF and FDCA yields (up to 4% and 1%, respectively)—which is due to the formation of by-products—and suggests routes for improvement.

Depleting reserves of fossil fuels and growing concerns with atmospheric CO_2 levels necessitate the development of non-petroleum derived, renewable fuels and carbon-based building blocks for chemical industries.[1] Solar[2] and biomass[3,4] refineries have been proposed as potential replacements for the current petroleum paradigm, and a key model reaction identified is the oxidation of biomass-derived[5,6] 2,5-hydroxylmethylfurfural (HMF) into 2,5-furandicarboxaldehyde (DFF) and 2,5-furandicarboxylicacid (FDCA), which are essential monomers for the production of biomass derived aromatic polyesters.[7]

The aerobic oxidation of HMF typically proceeds with precious metal heterogeneous catalysts such as Au, Pd, and Pt under strongly alkaline conditions (pH $\geq$ 13), high O_2 pressures (3–20 bar), and at elevated temperatures (30–130 °C).[8,9] An attractive alternative to these harsh conditions, besides using more mild conditions[10,11] or an enzyme-catalysed approach,[12] is electrochemical oxidation. HMF electro-oxidation on various anodes under mild conditions (in alkaline water at temperatures of 30–60 °C, and ambient O_2 pressure)[13–19] has been demonstrated. However, significant energy input, in the form of electricity is needed to drive this conversion.

Ideally, HMF electro-oxidation would be driven by renewable energy. Using a photoelectrochemical (PEC) cell[20] can afford a simple and direct route to exploit solar energy to both oxidize HMF (at a photoanode) and produce renewable fuels (*e.g.* H_2 from proton reduction) at a photocathode. This route also serves to overcome an important limitation of traditional PEC cells,[21] which oxidize water to form O_2. Indeed, given the slow kinetics of the oxygen evolution reaction (OER), replacing it with an alternative oxidation reaction can potentially improve the solar-to-fuel efficiency of PEC cells by lowering the operating potential of the anode.[22]

While the photocatalytic oxidation of HMF has been suggested,[23–25] the PEC oxidation of HMF to FDCA has been less developed. One recent report uses a $BiVO_4$ photoanode,[20] however the approach was severely limited since $BiVO_4$ is incapable of directly performing HMF oxidation. Instead, $BiVO_4$ first oxidizes a redox mediator (2,2,6,6-tetramethylpiperidine-1-oxyl, TEMPO) which then carries out the homogeneous oxidation of HMF in solution. This increases the complexity of product separation, and since TEMPO parasitically absorbs visible light,[26] it reduces sunlight harvesting by the photoelectrodes. Moreover, the problematic long-term stability of the TEMPO radical calls into question the practical application of this approach. Thus, the identification of a photoanode material that can directly oxidize HMF to FDCA, without redox mediators and selectively over water oxidation in aqueous electrolyte, is needed to advance the field.

Herein we demonstrate for the first time that WO_3 photoanodes can directly oxidize HMF in aqueous electrolyte under illumination while suppressing the competing water oxidation reaction. Our detailed analysis of the resulting product distribution and reaction kinetics gives important insights into the

Laboratory for Molecular Engineering of Optoelectronic Nanomaterials (LIMNO), École Polytechnique Fédérale de Lauanne (EPFL), Station 6, 1015 Lausanne, Switzerland. E-mail: kevin.sivula@epfl.ch

† Electronic supplementary information (ESI) available: Complete experimental details, Fig. S1–S8, and Table S1. See DOI: 10.1039/d0ra09989a

‡ These authors contributed equally to this work.

reaction pathways, suggesting routes to further enhance the performance.

Based on the unique PEC properties of WO_3, we hypothesized that it could provide advantages toward the direct photo-oxidization of HMF. Specifically, compared to $BiVO_4$, which has a valence band maximum (VBM) at a potential of 2.4 V *vs.* NHE,[27] the VBM of WO_3 is considerably more oxidizing at 3.1–3.2 V *vs.* NHE[27] suggesting an increased driving force to overcome the activation energy barrier associated with HMF oxidation. In addition, WO_3 also demonstrates poor selectivity for the OER, even in aqueous solution. In fact, WO_3 often prefers to oxidize other small molecules, or anions such as MeOH, and Cl^-.[25,28–31] This can reduce or eliminate competition from water oxidation when operating in aqueous conditions. This strategy has been employed in the past, where WO_3 was used to oxidize alcohols photoelectrochemically in aqueous solution.[32] Finally, WO_3 is easy to prepare and demonstrates stability in acidic aqueous media. These properties are highly desirable for a PEC material if it is to be employed in an H_2 producing PEC cell since acidic conditions favour the production of H_2 from water.

WO_3 photoanodes prepared by the sol–gel method (see ESI,† for details) were first examined for HMF oxidation in aqueous electrolyte using linear sweep voltammetry (LSV), and the results were compared to $BiVO_4$ and Fe_2O_3 (similar photoanode materials, for synthesis see ESI†). Fig. 1a–c shows LSV results in the dark and under simulated 1 Sun illumination, with and without 5 mM HMF in the electrolyte. We note that different pHs were used due to the stability limits of each material, thus all LSVs are plotted *versus* the reversible hydrogen electrode, RHE. We also note that HMF oxidation is favoured under basic conditions, which should be advantageous for $BiVO_4$ and Fe_2O_3.[5,14,16,17] However, while the current density, *J*, exhibits similar behaviour with and without HMF with $BiVO_4$ and Fe_2O_3 photoanodes, a clear difference is observed with WO_3. In a pH 4 electrolyte containing no HMF, WO_3 shows a photocurrent onset potential at 0.63 V *vs.* RHE and a saturated photocurrent density of 1.2 mA cm^{-2}. However, when 5 mM HMF is added to the solution, the onset potential shifts by −100 mV, and the saturated photocurrent density increases by 26% to 1.52 mA cm^{-2}. The unresponsiveness of $BiVO_4$ and Fe_2O_3 to HMF suggests that these photoanodes do not favour photo-oxidization of HMF over the OER, however the significant shift of the *J–E* curve observed with WO_3 suggests that WO_3 possesses a unique ability to oxidize the HMF substrate directly, and favourably compared to water oxidation. Although these results alone do not directly confirm either Fe_2O_3 or $BiVO_4$'s inability to oxidize HMF directly, other groups have demonstrated that $BiVO_4$ in particular is unable to perform this reaction on its own.[20] Furthermore, the marked J-E shift observed with the WO_3 suggests that the HMF is a kinetically easier substrate to oxidize. In this case, if a photoanode were capable of directly oxidizing this substrate, then we would expect to observe a cathodic shift in the photocurrent onset.

The remarkable ability of WO_3 to directly oxidise HMF was confirmed with rotating ring-disk electrode experiments (for Experimental details, and full explanation see ESI and Fig. S1†). Briefly, as seen in Fig. 1d, the ring current observed in the absence of HMF (due to the reduction of the O_2 formed at the WO_3 disk under illumination, see ESI† for additional discussion) is suppressed when HMF is added despite no significant change in the disk photocurrent, even at highly oxidizing potentials (1.43 V *vs.* RHE). This confirms that the photocurrent observed with HMF in Fig. 1c is due to HMF oxidation and not water oxidation when 5 mM HMF is present in the electrolyte.

The selectivity towards various HMF oxidation products and the durability of WO_3 was next examined *via* the continuous photo-oxidation of a 5 mM HMF electrolyte (aqueous NaPi buffer pH 4) under simulated solar illumination using a constant applied potential of 0.68 V *vs.* RHE in a 2-compartment cell (working and counter electrodes separated by a Nafion membrane) in order to eliminate the possibility of reducing oxidized products at the cathode. Larger-area photoelectrodes (*ca.* 3 cm^2 *vs.* 1 cm^2) and 3 Suns equivalent illumination were used to maximize the quantity of products formed. The concentration of HMF and the formed products were monitored using HPLC. Fig. 2a shows the evolution of the photocurrent and HMF concentration [HMF], over 64 h (data has been averaged from three independent runs). We note that the measured photocurrent was lower than expected from Fig. 1c due to the increased substrate resistance of the larger area photoanodes.[33,34] In addition, the photocurrent decreases from an initial 0.3 to 0.1 mA cm^{-2} over 64 h of continuous operation due to the depletion of oxidizable substrate (at the applied potential no photocurrent from the OER was observed in the absence of HMF). Indeed [HMF] decreased to *ca.* 200 μM. In contrast, only a 12% decrease in [HMF] was observed in a control experiment without WO_3 where the 5 mM HMF electrolyte was irradiated for 64 hours (see Fig. S2 and Table S1, ESI†). This small decease in

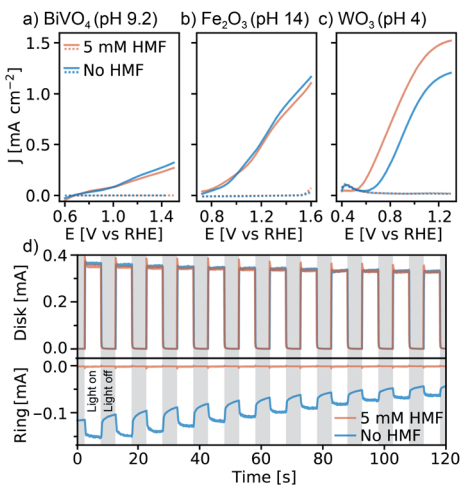

Fig. 1 Linear sweep voltammogram of (a) $BiVO_4$ photoanode in pH 9.2 NaBi buffer (+5 mM HMF), (b) α-Fe_2O_3 photoelectrode in pH 14 NaOH electrolyte (+5 mM HMF), and (c) WO_3 photoanode in pH 4 NaPi buffer (+5 mM HMF). The solid lines and dotted lines are LSVs under simulated 1 Sun illumination, and in the dark, respectively. The light illumination was from the back (glass) side. (d) Rotating ring-disk results: (top) WO_3 disk current at 1.43 V *vs.* RHE under intermittent illumination, (bottom) Pt ring current at 0.63 V *vs.* RHE (at these conditions O_2 is reduced to peroxide).

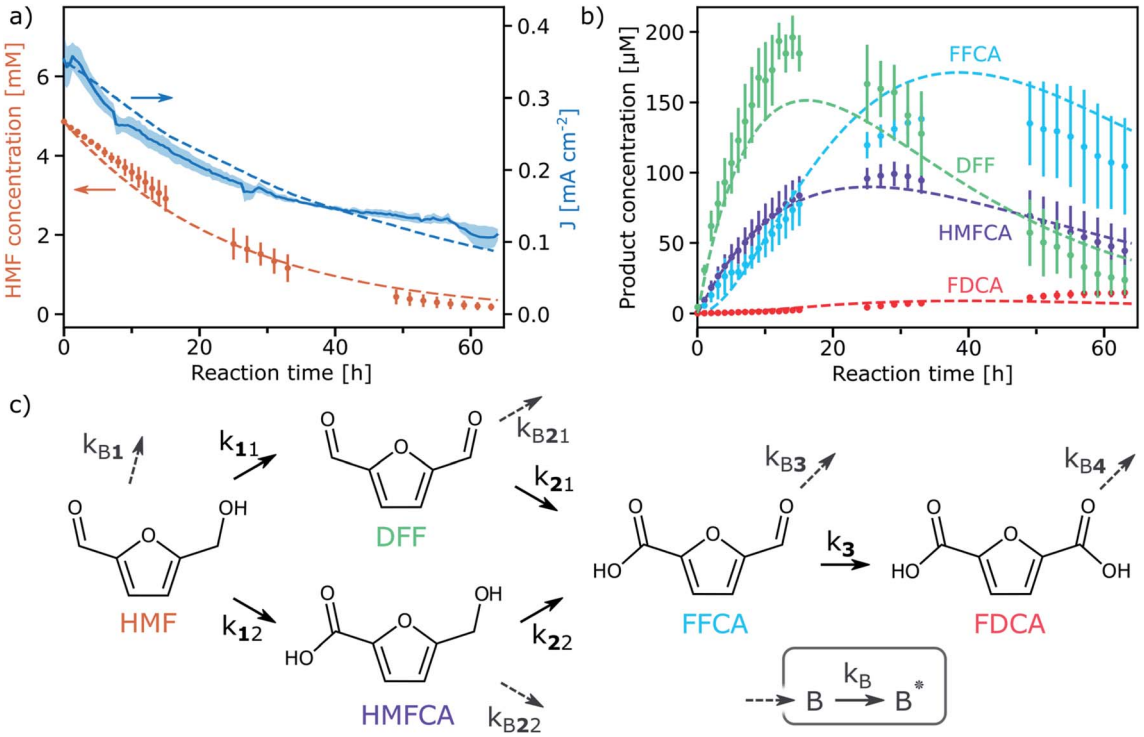

Fig. 2 Continuous photo-oxidation of HMF with WO_3 is shown by the evolution over time of: (a) the concentration of HMF and the photocurrent; (b) the concentration of DFF, HMFCA, FFCA and FDCA; the dashed lines are the result of the chemical kinetics fitting. Data is averaged over three independent runs and the error bars represent the standard deviation. (c) Reactions pathways for the formation of FDCA from HMF and by-product reactions leading to oxidized products B and B*.

[HMF] results from its photo-decomposition which has been reported previously.[14,35,36]

We note that no obvious corrosion of the WO_3 photoanode was observed *via* scanning electron microscopy during extended operation (see Fig. S3, ESI†). This confirms the stability of the anode under these operation conditions.

The detected products formed during the continuous photo-oxidation with WO_3 are shown in Fig. 2b. 2,5-furandicarboxaldehyde (DFF), 5-hydroxymethyl-2-furan-carboxylic acid (HMFCA), 5-formyl-2-furancarboxylic acid (FFCA), and 2,5-furandicarboxylic acid (FDCA) are observed. It appears that DFF and FFCA are the primary products, with DFF being formed first at yields up to 4% (based on HMF), while FFCA and finally FDCA appear later, as expected from the established oxidation pathways[37] (Fig. 2c). While the FDCA concentration is still slightly increasing after 64 hours, its yield is quite modest (*ca.* 25 μM, 0.5% based on HMF), and raises important questions about the reaction pathways and reaction kinetics occurring during the direct oxidation at the photoanode. Indeed, we note that the amount of consumed HMF is not equivalent to the amount of produced DFF and HMFCA. Moreover, the FDCA production rate appears smaller than the FFCA oxidation rate. This implies that side reactions involving the HMF and the other small molecules is occurring. We note that the formation of macromolecular humin by-products has been previously reported to occur with HMF oxidation.[38]

Given the relatively complex reaction pathways, the limited yield of FDCA compared to the other products, and the possible production of macromolecular by-products, we next developed a model of the photo-electrochemical oxidation reactions. The set of differential equations describing the evolution of the concentration of the reactants/products and an equation for the photocurrent were solved numerically and fit with pseudo first order reaction rate constants, k's, defined in Fig. 2c (see ESI† for full details and explanation). Briefly, we considered that the concentration of photogenerated holes at the WO_3 surface to be in excess, and that mass transfer from the bulk of the electrolyte to the surface of the photoanode to be similar for all components (see Fig. S4 and S5, ESI†). To obtain reasonable rate constant fitting, we accounted for the formation of unknown oxidation by-products, B, by the oxidation of the known products, and the further oxidation of these species (into B*), as shown in Fig. 2c, which is consistent with the formation of macromolecular oxidation products. The simulated photocurrent and product concentrations from the fit model are shown as dashed lines in Fig. 2a and b, and the obtained reaction rate constants (shown in Table 1) with given standard error show a high-quality fit. Moreover, these values give quantitative insight to the oxidation pathways on the WO_3 photoanode. Since the rate constant for DFF production (k_{11}) is 2.5 times larger than for HMFCA production (k_{12}), it appears that the oxidation of HMF to DFF is preferred. This result is corroborated by LSV performed with only HMF, DFF, or the diol, 2,5-bis(hydroxymethyl)furan (BHMF), which shows a higher photocurrent for HMF or BHMF compared to DFF, implying that WO_3 reacts faster with the alcohol moiety (see Fig. S6,

Table 1 Pseudo-first order rate constants for oxidation by WO_3 photoanode at 0.68 V *vs.* RHE (pH 4, 3 Sun illumination), as extracted from model fitting (see reactions Fig. 2c)

	Rate constant[a] ($\times 10^{-3}$ h^{-1})		Rate constant[a] ($\times 10^{-3}$ h^{-1})
k_{11}	5.54 (0.19)	k_{B1}	30.2 (0.4)
k_{12}	1.82 (0.05)	k_{B21}	43.5 (7.1)
k_{21}	64.9 (4.1)	k_{B22}	0.03 (8.4)
k_{22}	38.0 (8.5)	k_{B3}	54.5 (4.3)
k_3	7.30 (0.39)	k_{B4}	72.2 (5.9)
		k_B	1.73 (0.27)

[a] Standard error from fitting the averaged experimental data in parentheses.

ESI†). Furthermore, for both pathways to produce FDCA, it appears that the initial HMF oxidation is the rate limiting step as k_3, k_{21}, and k_{22} are all larger than k_{11} and k_{12}.

Regarding the formation of unknown by-products, this generally occurs faster than oxidation by the known pathways. For example, the oxidation of HMF to either DFF or HMFCA is 4 times slower than the oxidation of HMF to the likely humin by-products. As an exception, the oxidation of HMFCA to FFCA occurs relatively fast (k_{22}) compared to its competing oxidation to by-product (k_{B22}). This suggests that FDCA yield may be improved by driving the reaction through the HMFCA pathway. Finally, we note that the desired FDCA product is further oxidized at the WO_3 surface (as verified by LSV, Fig. S7, ESI†), and this by-product reaction appears to occur with the fastest rate constant. Thus, the low FDCA yield is in part due its quick oxidation with the photogenerated holes at the WO_3 surface. Overall, it is clear that identifying strategies to reduce the rate of the by-product reactions (*i.e.* by adding a selective surface catalyst) will be needed to further advance the direct PEC production of FDCA.

Conclusions

In summary, we demonstrate the first example of direct PEC oxidation of HMF to DFF and FDCA. The unique reactivity of WO_3, including its known poor selectivity for the OER and stability in aqueous acidic electrolyte are likely contributing factors towards its unique ability to directly photo-oxidize HMF under aqueous conditions, while suppressing the water oxidation reaction. A maximum yield of DFF up to *ca.* 4% was observed under prolonged operation, and although yields of FDCA remain modest at < 1%, modelling the reaction kinetics suggests that increasing the rate of intermediate HMFCA production and reducing the unwanted oxidation by-products can lead to further improvements. Overall, this demonstration represents an important simplification over previous work and progresses PEC systems towards the scalable and economical production of both solar fuels and valorized biomass products—without requiring the sluggish OER.

Conflicts of interest

There are no conflicts to declare.

Acknowledgements

The authors acknowledge support from the Swiss Competence Centre for Energy Research (SCCER Heat and Electricity Storage, contract #CTI 1155002545). N. P. thanks the Royal Thai Government for a scholarship.

References

1 S. J. Davis, N. S. Lewis, M. Shaner, S. Aggarwal, D. Arent, I. L. Azevedo, S. M. Benson, T. Bradley, J. Brouwer, Y.-M. Chiang, C. T. M. Clack, A. Cohen, S. Doig, J. Edmonds, P. Fennell, C. B. Field, B. Hannegan, B.-M. Hodge, M. I. Hoffert, E. Ingersoll, P. Jaramillo, K. S. Lackner, K. J. Mach, M. Mastrandrea, J. Ogden, P. F. Peterson, D. L. Sanchez, D. Sperling, J. Stagner, J. E. Trancik, C.-J. Yang and K. Caldeira, *Science*, 2018, **360**, eaas9793.
2 J. A. Herron, J. Kim, A. A. Upadhye, G. W. Huber and C. T. Maravelias, *Energy Environ. Sci.*, 2015, **8**, 126–157.
3 A. J. Ragauskas, G. T. Beckham, M. J. Biddy, R. Chandra, F. Chen, M. F. Davis, B. H. Davison, R. A. Dixon, P. Gilna, M. Keller, P. Langan, A. K. Naskar, J. N. Saddler, T. J. Tschaplinski, G. A. Tuskan and C. E. Wyman, *Science*, 2014, **344**, 1246843.
4 J. Ruiz, G. Olivieri, J. de Vree, R. Bosma, P. Willems, J. H. Reith, M. H. M. Eppink, D. M. M. Kleinegris, R. H. Wijffels and M. J. Barbosa, *Energy Environ. Sci.*, 2016, **9**, 3036–3043.
5 R.-J. van Putten, J. C. van der Waal, E. de Jong, C. B. Rasrendra, H. J. Heeres and J. G. de Vries, *Chem. Rev.*, 2013, **113**, 1499–1597.
6 A. H. Motagamwala, K. Huang, C. T. Maravelias and J. A. Dumesic, *Energy Environ. Sci.*, 2019, **12**, 2212–2222.
7 Y. Zhu, C. Romain and C. K. Williams, *Nature*, 2016, **540**, 354–362.
8 Z. Zhang and K. Deng, *ACS Catal.*, 2015, **5**, 6529–6544.
9 I. Delidovich, K. Leonhard and R. Palkovits, *Energy Environ. Sci.*, 2014, **7**, 2803.
10 B. Liu, Y. Ren and Z. Zhang, *Green Chem.*, 2015, **17**, 1610–1617.
11 J. An, G. Sun and H. Xia, *ACS Sustainable Chem. Eng.*, 2019, **7**, 6696–6706.
12 W. P. Dijkman, D. E. Groothuis and M. W. Fraaije, *Angew. Chem., Int. Ed.*, 2014, **53**, 6515–6518.
13 B. You, N. Jiang, X. Liu and Y. Sun, *Angew. Chem., Int. Ed.*, 2016, **128**, 10067–10071.
14 S. R. Kubota and K.-S. Choi, *ChemSusChem*, 2018, **11**, 2138–2145.
15 A. Villa, M. Schiavoni, S. Campisi, G. M. Veith and L. Prati, *ChemSusChem*, 2013, **6**, 609–612.
16 W.-J. Liu, L. Dang, Z. Xu, H.-Q. Yu, S. Jin and G. W. Huber, *ACS Catal.*, 2018, **8**, 5533–5541.
17 K. R. Vuyyuru and P. Strasser, *Catal. Today*, 2012, **195**, 144–154.
18 R. Latsuzbaia, R. Bisselink, A. Anastasopol, H. van der Meer, R. van Heck, M. S. Yagüe, M. Zijlstra, M. Roelands,

M. Crockatt, E. Goetheer and E. Giling, *J. Appl. Electrochem.*, 2018, **48**, 611–626.
19 A. R. Poerwoprajitno, L. Gloag, J. Watt, S. Cychy, S. Cheong, P. V. Kumar, T. M. Benedetti, C. Deng, K. Wu, C. E. Marjo, D. L. Huber, M. Muhler, J. J. Gooding, W. Schuhmann, D. Wang and R. D. Tilley, *Angew. Chem., Int. Ed.*, 2020, **59**, 15487–15491.
20 H. G. Cha and K.-S. Choi, *Nat. Chem.*, 2015, **7**, 328–333.
21 Y. Chen, X. Feng, Y. Liu, X. Guan, C. Burda and L. Guo, *ACS Energy Lett.*, 2020, **5**, 844–866.
22 C. R. Lhermitte and K. Sivula, *ACS Catal.*, 2019, **9**, 2007–2017.
23 I. Krivtsov, E. I. García-López, G. Marcì, L. Palmisano, Z. Amghouz, J. R. García, S. Ordóñez and E. Díaz, *Appl. Catal., B*, 2017, **204**, 430–439.
24 V. R. Battula, A. Jaryal and K. Kailasam, *J. Mater. Chem. A*, 2019, **7**, 5643–5649.
25 K. D. McDonald and B. M. Bartlett, *RSC Adv.*, 2019, **9**, 28688–28694.
26 V. A. Koptyug, in *Atlas of Spectra of Aromatic and Heterocyclic Compounds*, 1982, vol. 24, p. 105.
27 J. C. Vedrine, *Metal Oxides in Heterogeneous Catalysis*, Elsevier, 2018.
28 C. R. Lhermitte, J. G. Verwer and B. M. Bartlett, *J. Mater. Chem. A*, 2016, **4**, 2960–2968.
29 Q. Mi, A. Zhanaidarova, B. S. Brunschwig, H. B. Gray and N. S. Lewis, *Energy Environ. Sci.*, 2012, **5**, 5694–5700.
30 J. C. Hill and K.-S. Choi, *J. Phys. Chem. C*, 2012, **116**, 7612–7620.
31 H. Tateno, S. Iguchi, Y. Miseki and K. Sayama, *Angew. Chem., Int. Ed.*, 2018, **57**, 11238–11241.
32 O. Tomita, T. Otsubo, M. Higashi, B. Ohtani and R. Abe, *ACS Catal.*, 2016, **6**, 1134–1144.
33 X. Yao, D. Wang, X. Zhao, S. Ma, P. S. Bassi, G. Yang, W. Chen, Z. Chen and T. Sritharan, *Energy Technol.*, 2018, **6**, 100–109.
34 S. Hernández, G. Gerardi, K. Bejtka, A. Fina and N. Russo, *Appl. Catal., B*, 2016, **190**, 66–74.
35 L. Filiciotto, A. M. Balu, A. A. Romero, C. Angelici, J. C. van der Waal and R. Luque, *Mol. Catal.*, 2019, **479**, 110564.
36 S. K. R. Patil, J. Heltzel and C. R. F. Lund, *Energy Fuels*, 2012, **26**, 5281–5293.
37 P. Verdeguer, N. Merat and A. Gaset, *J. Mol. Catal.*, 1993, **85**, 327–344.
38 M. Kim, Y. Su, A. Fukuoka, E. J. M. Hensen and K. Nakajima, *Angew. Chem., Int. Ed.*, 2018, **57**, 8235–8239.